Journal of Fluids and Structures (2000) **14,** 613–634
doi:10.1006/jfls. 2000.0287, available online at http://www.idealibrary.com on IDEAL®

THE SIMULATION OF CORIOLIS METER RESPONSE TO PULSATING FLOW USING A GENERAL PURPOSE F.E. CODE

A. Belhadj, R. Cheesewright and C. Clark

Department of Systems Engineering, Brunel University
Uxbridge, Middlesex UB8 3PH, United Kingdom

(Received 14 December 1998, and in final form 16 November 1999)

The publication of a theoretical analysis of the response of a simple straight-tube Coriolis meter to flow pulsations raised the question of the extent to which the results of that analysis are generic over the wide range of geometric configurations used in commercially available meters. A procedure for using a general purpose finite element (FE) code to investigate this question is presented. The dual time scales, which are an essential feature of pulsating flow through a Coriolis meter, are used to minimize the amount of computation required to simulate the meter response. The FE model is developed in a full 3-D form with shear deflection and axial forces, and the computation of the simulated response for the geometrically most complex meter currently available shows that this level of representation is necessary to reveal the full details of the response. The response derived from the FE simulation for straight-tube meters, is compared with the published theoretical response and to experimental data. Over a range of different meters, the characteristics of the sensor signals in the presence of flow pulsations are shown to be generally similar. In all cases, the simulated sensor signals contain components corresponding to beating between the pulsation frequency and the meter drive frequency, in addition to the main component at the drive frequency. Spectra are computed from the simulated meter responses and these are used to show that the relationship between the mass flow rate and the phase difference between the component of the sensor signals at the drive frequency, is not significantly affected by the pulsations. Thus, the work suggests that the reports of changes in meter calibration due to certain frequencies of flow pulsation represent errors in signal processing rather than fundamental changes in the meter characteristics.

1. INTRODUCTION

Due to their high accuracy (typical uncertainty for liquids $< 0{\cdot}1\%$ full scale) and wide applicability, Coriolis mass flow meters have become widely used in industry. They measure the mass flow by vibrating a fluid conveying tube at a resonant frequency (commonly, but not always, the lowest mode frequency). As the tube oscillates, directional changes in the moving fluid are induced and, as a result, Coriolis forces are developed. The effect of these forces on the flow tube produces a distortion of the driven motion. The distortion has the shape of a higher vibration mode but it occurs at the drive frequency. The resonant frequency corresponding to the distortion mode shape is called the Coriolis frequency. Meters typically have two displacement detectors mounted at different points along the flow tube, and the effect of the distortion is to produce a phase shift between the signals from the two detectors, which, for steady flow, is linearly proportional to the mass flow rate.

Coriolis meters may have a single tube or a balanced pair of tubes and the tubes may be straight or of quite complex shapes; a good overview of the possibilities is given in the

0889–9746/00/070613 + 22 $35.00/0

survey paper by Baker (1994). The driven motion is usually designed to be of constant amplitude, using feedback from one or both of the displacement detectors. The exact nature of the feedback, as well as the method used to determine the phase difference (and hence the mass flow rate) from the detector signals, vary from one manufacturer to another and were not available to the authors. For a steady fluid flow the signals from the detectors will contain only one significant frequency component, since both the driven motion and the Coriolis distortion are at the same frequency. Thus, there is no inherent difficulty in the determination of the phase difference between the signals. However, if a pulsatile component in the flow introduces significant additional components in the tube motion and hence in the detector signals, at frequencies other than the drive frequency, then at least two important questions are raised. Firstly, do these additional components change the linear relationship between the phase difference of the components at the drive frequency and the mass flow rate? Secondly, how well do meters handle detector signals with multiple frequency components? Details of the different algorithms used by the various manufacturers to extract the phase difference between the sensor signals were not available to the authors, and so this second question could only be examined experimentally. Results of a parallel experimental study have been reported by Cheesewright, Clarke and Bisset (1999). The present work is part of an attempt to answer the first question and at the same time to predict the characteristics of the additional components of tube motion.

There have been only two significant publications dealing with the effect of flow pulsations on Coriolis meters. Vetter and Notzon (1994) reported the results of experiments involving two different U-tube meters subjected to pulsations from a piston pulsator and from a gear pump. They reported irregular meter output signals with pulsations at the drive frequency and large meter errors with pulsations at the Coriolis frequency. Cheesewright and Clark (1998) reported the results of an analytical solution to the problem, for a simple straight tube meter. This analysis suggested that, in the presence of flow pulsations, the detector signals could contain components at four different frequencies, namely, the drive frequency, the Coriolis frequency and frequencies corresponding to the sum and difference of the drive frequency and the pulsation frequency. However, this work also suggested that the relationship between the component of the detector signals at the drive frequency, and the mass flow rate through the meter, was not affected by the pulsations. The complexity of the analysis reported by these authors is such that an extension of the work to include the more complex geometries, typical of current, commercially available meters, would be very difficult or even impossible.

2. FINITE ELEMENT SOLUTIONS

It would, at least in principle, be possible to solve the problem by fully coupling FE solutions for the fluid flow within the meter tube and for the tube structure. An example of the application of this approach, to the relatively simple problem of the dynamic response of an initially straight but flexible pipe conveying a fluid, has been reported by Olson & Jamison (1997), but the extension of this approach to complex three-dimensional geometries would be unrealistically demanding of computing time. Païdoussis & Li (1993) and Tijsseling (1996) have published reviews of work on fluid–structure interactions, including both the development of special (FSI) codes and the use of existing commercial FE codes.

For cases where only the structural response of the tube to the flow body forces is of interest (i.e. detailed behaviour of the flow is of no interest), a simplified alternative approach can be adopted. In this approach the tube is idealized by using simple beam elements loaded both by structural forces (applied, inertia, stiffness and damping) and by

fluid forces (inertia, centripetal and Coriolis). Commercially available Coriolis meter tubes are made up of straight sections of tube joined by curved sections (see Figure 4) so that ideally, curved beam elements should be used, with each element being characterized by a radius of curvature. However, examination of the equations for a curved beam element, as derived, for example, by Sultan and Hemp (1989), shows that when a curved beam element is approximated by a large number of short straight elements, the accuracy with which the fluid/tube interaction is modelled increases rapidly as the number of straight elements is increased. There are small residual errors in the modelling of the forces on the tube, but these errors predominantly involve "in-plane" forces, and both the driven motion of the meter tubes and the additional motions that are the subject of this work are "out-of-plane". The concentration on "out-of-plane" motions also allows the neglect of any consideration of the extension of the tube centreline [see Misra, Païdoussis & Van (1988a, b)].

On the basis of the above factors it was decided to follow the work of Stack, Garnett and Pawlas (1993) and model the meters in terms of straight beam elements. This allowed the equations governing the motion of a tube element (and the enclosed fluid) to be derived and an appropriate FE code used to solve these equations for the ensemble of elements comprising the meter. This approach kept the amount of computation within reasonable bounds, while achieving the objective in the present work, which was to predict the structural dynamic response of the meter tubes (and hence the characteristics of the signals from the displacement sensors).

There have been several reports of the application of this approach to problems involv-–ing *steady flow* through a Coriolis meter. Stack *et al.* (1993) used a simplified Timoshenko beam representation of the tube element, and Hulbert, Darnell and Brereton (1995) extended the work to include the effects of axial tension. For these steady flow problems the governing equations are of complex eigenvalue form and general purpose FE codes are available to solve such problems. Both these publications reported comparisons of predicted drive frequencies (including the small flow rate dependence) and meter calibration factors, with those obtained by experiment for commercially available meters. In both cases, the agreement was within 5%, with the latter paper reporting slightly better agreement.

The present work differs from these previous studies, because the presence of the flow pulsations changes the governing equations from a complex eigenvalue form to a form in which the spatial and temporal variables are not separable. This can easily be deduced from the presence of two, independent, externally imposed time scales, namely the drive frequency and the pulsation frequency. A consequence of this difference is that an FE solution must either take a dynamic form, stepping forward in time until an asymptotic, fully developed motion is reached, with the sensor signal characteristics determined from temporal averages (at that condition), or the solution must be developed via a modal decomposition along similar lines to those used by Cheesewright and Clark (1998). It is not obvious, however, that the latter approach can be easily integrated with the applicability to complex geometries which characterizes modern general purpose FE codes. It was therefore decided to adopt the dynamic FE calculation approach.

Although in general the spatial and temporal variables are not separable, if the time step associated with the dynamic FE calculation is much smaller than either the time scale of the highest structural vibration mode of interest or that of the fluid pulsations, separability can be assumed for each time step. This, as will be demonstrated in Section 3, leads to a formulation of the equations for an FE solution, which are of a "standard" form except that the stiffness and damping matrices are time dependent. It would be possible to develop a program which evaluated these matrices at every (FE) time step. An FE solution set up in

this way would still involve a very large computational effort, and so a further approximation was introduced, which took advantage of the two time scales noted above and of a feature of the ANSYS FE code. The matrices were only updated at intervals, which gave an adequate representation of the pulsation waveform, and were kept constant during the large number of FE time steps which occurred during these intervals. Furthermore, the differing matrices were introduced via the "births and deaths of elements" feature of the code so that they only needed to be evaluated for one cycle of the pulsation, even though the dynamic FE calculation had to be extended over a large number of such cycles to reach the asymptotic state.

The approximations noted above made it desirable that the FE treatment should be validated and this was achieved by comparison with the solutions published by Cheesewright and Clark (1998) for a simple straight tube meter. However, the overall objective of the present FE work was to develop a technique which was economical with respect to computer time and which could be relatively easily applied to any of the commercially available Coriolis meters. As will be demonstrated in Section 5, although the drive is always in one plane, for some of the meters the geometry is so complex that a full three-dimensional analysis is necessary to give an adequate representation. Thus, the development of the FE equations was performed for the three-dimensional case, using Timoshenko beam elements without any simplifications.

3. GENERAL FINITE ELEMENT EQUATIONS OF MOTION

The FE solution adopted to analyse the dynamic behaviour of Coriolis meters is based on a pure structural engineering approach. Thus, conceptually, the effect of the pulsating flow on the vibrating tube is seen as similar to the effect of a vehicle moving with variable speed on a bridge. In the formulation of the fluid-conveying beam element the fluid flow is assumed to be approximated as a plug flow. The wavelength of the flow pulsation is assumed to be large compared with the meter length. Thus, the fluid is treated as a solid mass travelling along the tube at a uniform but time-varying speed. Also, the fluid and the tube are assumed to be perfectly coupled by having equal displacements and rotations. The assumption of equal rotations of the tube and the fluid is an approximation, since the true rotation of the fluid will be somewhere between zero (inviscid fluid) and that of the tube. The error introduced by this approximation will be small because the rotational inertia of the fluid is never more than 25% of that of the tube.

The meter is considered to be made up of straight fluid-tube finite elements having length L and six degrees of freedom per node (three translations and three rotations). The distributed mass of fluid moves continuously without separating from the tube element, and travels at time-varying velocity $V = V(t)$. A Timoshenko beam formulation is adopted for the element. This takes into account effects of shear and rotary inertia in the transverse deflection of the tube element. Thus, the equations expressing the transverse displacement u, the flexural rotation θ and the shear strain ϕ, in the $\{x, y\}$ plane, in terms of the distance along the tube x and the time t, together with the material properties of the tube and the fluid, can be obtained by recasting the analysis for a time-dependent flow reported by Païdoussis & Issid (1974), into the form used by Stack, *et al.* (1993). The resulting equations are:

$$(m_p + m_f)\frac{\partial^2 u}{\partial t^2} + 2m_f V\frac{\partial^2 u}{\partial x \partial t} + m_f V^2\frac{\partial^2 u}{\partial x^2} + m_f(L - x)\frac{\mathrm{d}V}{\mathrm{d}t}\frac{\partial^2 u}{\partial x^2} - kGA_p\left(\frac{\partial^2 u}{\partial x^2} - \frac{\partial \theta}{\partial x}\right) = 0,$$

$$(m_p r_p^2 + m_f r_f^2)\frac{\partial^2\theta}{\partial t^2} - EI_p\frac{\partial^2\theta}{\partial x^2} - kGA_p\phi = 0,$$

$$\phi = \frac{\partial u}{\partial x} - \theta. \tag{1}$$

It should be noted that the derivation of equations (1) differs from the derivation of the equivalent equation given by Cheesewright and Clark (1998) in that it includes the effects of axial tensions, even though the tension does not appear explicitly in the equations [the tension has been eliminated by substitution from a force/momentum balance in the x-direction; see Païdoussis (1998) for details]. Closely similar equations can be written for the lateral displacement, the flexural rotation and the shear strain in the $\{x, z\}$ plane.

By assuming that, over a short period of time (as indicated in Section 2) the space and time variables are separable, the FE development described, for example, by Stack *et al.* (1993) can be applied to these equations as described briefly in Appendix A. This leads to a standard matrix form of the dynamic equation of motion which can be written as

$$M\frac{\mathrm{d}^2 q}{\mathrm{d}t^2} + B\frac{\mathrm{d}q}{\mathrm{d}t} + Kq = 0, \tag{2}$$

where q is the vector of nodal displacements and rotations, and M, B and K are the element matrices (given in detail in Appendix A). The element stiffness and damping matrices K and B, contain terms depending on the flow velocity $V = V_0(1 + \alpha \sin \omega_p t)$ and on $\mathrm{d}V/\mathrm{d}t$), and are thus time-dependent.

FE codes are designed to solve systems of equations like equation (2) above, with one equation for each of the relevant planes. Alternatively the equations for the $\{x, y\}$ and $\{x, z\}$ planes can be combined with a simple axial tension/axial displacement equation for the $\{y, z\}$ plane to give a single 3-D matrix equation and, as indicated in Appendix A, this was the route taken in the present work. For constant element matrices the solution will yield resonant frequencies and the associated distributions of displacements and rotations over the whole structure. When the element matrices are time-dependent, only a transient solution is possible, starting from an initial distribution of displacements and rotations and tracing out the changes of these distributions with time. The time step, which can be used in a transient solution, is dictated by the highest frequency component which it is desired to resolve. As pointed out in Section 2, the evaluation of the time-dependent element matrices at every time step would involve an excessively large amount of computation. In order to avoid this unnecessary computational overhead, it was established by preliminary computations that 16 time steps were sufficient to establish the characteristics of the pulsation cycle, so that the time-dependent matrices only needed to be computed 16 times and could then be repeated for successive pulsation cycles. The computational time scale was chosen to be $\leq 1/[20(f_1 + f_p)]$ and $= 1/[16nf_p]$, where f_1 is the meter drive frequency, f_p is the flow pulsation frequency, and n is an integer, thus giving at least 20 time steps over the period of the highest frequency of interest. A representation of this dual time step procedure is shown in Figure 1.

4. SOLUTION USING ANSYS

4.1. Implementation of the Solution

The FE code which was available for this work was ANSYS. While it would have been possible to have incorporated the problem specification (for a range of very different meter geometries), and the dual time step concept described above, by programming around the

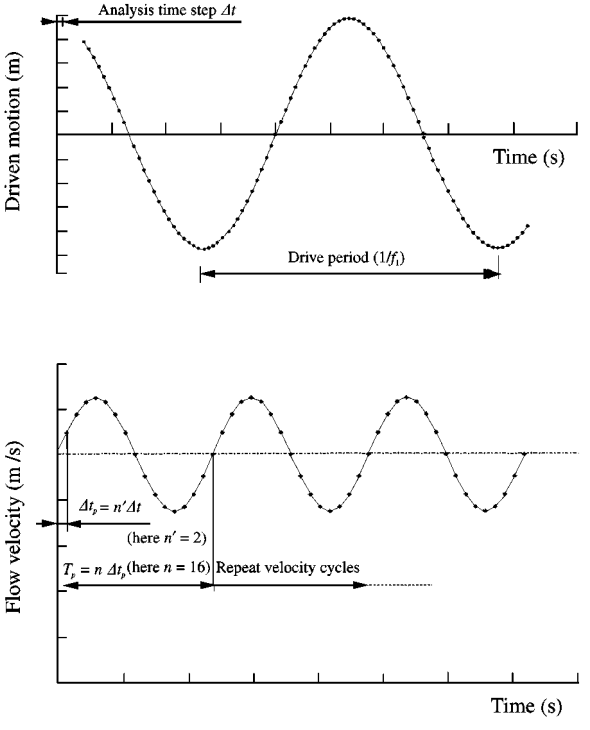

Figure 1. Illustration of the two different time steps used in the solution.

basic core of the code, it proved to be more efficient to utilize the following special features of the code:

(i) the Matrix27 element, which represents an arbitrary (12×12) 3-D element whose geometry is undefined but whose elastic kinematic response can be specified by stiffness, damping or mass coefficients, allowed the matrix elements given in Appendix A to be read into ANSYS;

(ii) the element "birth and death" feature, which provides a simple method to activate and de-activate selected elements in the FE model, allowed the 16 steps of the pulsation cycle to be set up as parallel elements and switched in and out as the cycle proceeded;

(iii) the parametric design language feature of ANSYS allowed the above procedures to be implemented very simply via an input file which could be used repeatedly.

In the form in which the element "birth and death" feature is implemented in ANSYS, it causes an element which is activated (or re-activated) to go immediately from the unstressed state to the fully stressed state; this introduced undesirable transients in the solution. This problem was overcome by dividing the element matrices into a time-independent (steady) part and a time-dependent part, having 17 elements in parallel: one, which was always active, containing the steady part, and the other 16, which were switched in and out in turn and which contained the time-dependent parts appropriate to the particular point in the pulsation cycle. In order to avoid elements with a negative stiffness matrix it was necessary to retain a small part of the steady-state matrices in the time-dependent elements. Figure 2 shows a diagrammatic representation of the switching process.

In setting up the details of the input of the element matrices it was necessary to decide on the approximation to be used with regard to the $\mathrm{d}V/\mathrm{d}t$ terms which appear in the stiffness

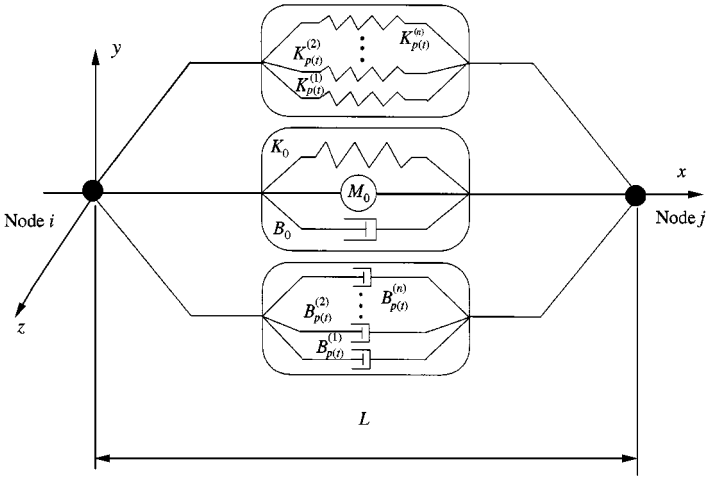

Figure 2. Representation of the coordinate system and the switching process using parallel elements. M_0, B_0 and K_0 are the constant element matrices for a tube conveying steady flow at (mean) velocity, $V = V_0$; $B_{p(t)}^{(n)}$ and $K_{p(t)}^{(n)}$ are the time-dependent element matrices resulting from time dependent velocity component; n (1 to 16) indicates the position in the pulsation velocity cycle.

matrix (see Appendix A). Initial solutions were performed with these terms set to zero, but later they were evaluated as the mean temporal gradient over the appropriate pulsation time step. For geometrically simple meters no differences could be detected between the two solutions, but for the more complex meters there were small differences.

4.2. Initial Conditions

The theoretical solutions reported by Cheesewright and Clark (1998) assumed that the meter was being driven with zero flow and then the flow (either steady or pulsating) was suddenly started. This would not have been easy to implement in the FE solution, so it was decided to start the transient solutions from a condition corresponding to steady flow (at a velocity corresponding to the mean velocity of the pulsating flow). Unfortunately, the ANSYS code available for this work did not contain a complex eigenvalue solver, which could accommodate the type of elements used in this work. Thus, it was necessary to start from an eigenvalue solution in which the fluid velocity terms were retained in the stiffness matrix but the damping matrix was assumed to be zero. This solution gave the "correct" modal frequencies for the chosen flow rate, i.e. it included the very small flow-rate dependence of the modal frequencies which has been demonstrated by Cheesewright and Clark (1998), Stack, *et al.* (1993) and others. It did not however, include the asymmetries associated with the Coriolis forces. When the distribution of tube displacements corresponding to the driven mode of the meter were taken from the eigenvalue solution and used to start a transient solution, it was found that the imperfections in these starting conditions introduced additional frequency components in the computed motion. These additional frequency components decayed as the transient solution proceeded, and a very long run confirmed that they were a result of the starting conditions and that they disappeared after a sufficiently long time.

The computations were performed on a dual Pentium Pro machine with 256 MB of memory, under the Windows NT4 operating system, and the run times were of the order of days, particularly for the geometrically more complex meters. In order to reduce the

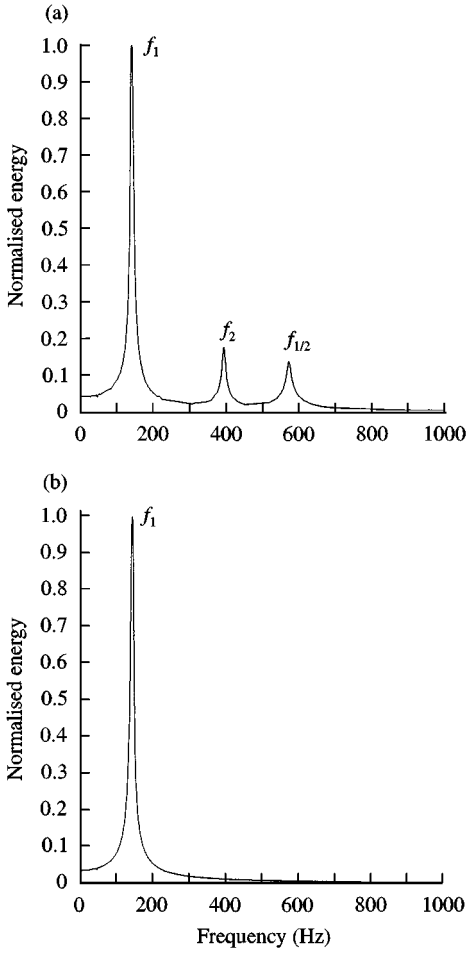

Figure 3. Spectrum of simulated sensor signal for steady flow (with drive removed): (a) during initial transient; (b) for steady state.

computational overhead of the imperfect initial conditions, the main computations were performed in two parts. First a relatively long run was made with a high numerical damping (10 times the default ANSYS value) to eliminate the spurious frequency components, and then the output of that run was used to start a run using the default value of the numerical damping. Figure 3(a) shows a spectrum of the tube displacements (at a sensor position) derived from the solution near the beginning of the highly damped part of the solution, and Figure 3(b) shows the corresponding spectrum derived from the subsequent run, with default damping. These spectra were taken from a solution for steady flow through a simple, straight-tube meter, and additional peaks on the spectrum from the early stages of the solution correspond to the Coriolis frequency and the first modal frequency of a tube of length $L/2$ (the half-beam frequency). The presence of the spectral peak at the Coriolis frequency corresponds to the term at this frequency predicted by Cheesewright and Clark (1998), arising from initial conditions. Because the term arises from initial conditions and there is no subsequent energy input to it, the term will decay under the influence of damping, so that the spectrum from the subsequent run shows only the drive frequency.

Because of the necessity of having a minimum level of numerical damping (the default damping), any transient solution would show a decay with time if the motion was not driven. Commercially available meters are driven by a feedback system, based on one or both of the sensor signals, and designed to keep the amplitude of the driven motion constant. It was not possible to directly simulate this drive because the feedback system differs from one manufacturer to another and details of the systems were not available to the authors. The FE computations were driven by requiring that the motion of the central node was of the form $U_d = U_0 \cos(\gamma_1 t)$, where U_0 was taken as 0·2 mm. It was appreciated that this form of drive will tend to reduce the occurrence of third or higher odd modes in the computed motion, but such a constraint is in keeping with the predictions of Cheesewright and Clark (1998).

4.3. Presentation of Results

The Introduction identified two objectives for this work which were the determination of any additional components in the motion of the sensors due to flow pulsations and the examination of the question as to whether the flow pulsations change the linear dependence of the phase difference between the component of the sensor signals at the drive frequency and the mass flow rate. In order to answer the first question, the solution is used to create a digital time history of the displacement of a sensor and then the periodogram technique (Bendat & Piersol 1971) is used to generate a spectrum from this time history. Relevant additional components of motion may be as small as the Coriolis component and hence may be of the order of 10^{-3} times the component at the drive frequency. In order to emphasize the presence of the additional components, the majority of the spectra are presented in terms of the spectrum of the difference between the time history for the pulsating flow and the time history for a steady flow with the same mean velocity. This representation is only possible because the two time histories are derived from computations which start from the same point in time, run for exactly the same length of time, and are driven at the same frequency and amplitude.

Ideally, the answer to the second question would have involved the application of a digital bandpass filter, centred on the drive frequency (f_1), to the time histories of the computed sensor motions and then the determination of the phase (or time) difference between the two filtered signals. In practice, it proved to be impractical to generate sufficiently long computed records of the sensor motions to yield accurate filtered signals. However, the absence of a peak at the drive frequency (f_1) in the spectrum of the difference between the time histories for a pulsating flow and the corresponding steady flow is an equally good proof that the dependence of the phase difference between (i) the components of the sensor signals at the drive frequency and (ii) the mass flow rate is independent of the presence of flow pulsations.

In a simulation of the signal processing used in some earlier commercial meters, the time difference between the two sensor signals was calculated for each pair of zero crossings of the computed signals, with the exact positions of the zero crossings being established by interpolation. These time differences were averaged over an integer number of cycles of the drive signal (two estimates per cycle). Typically, the "steady-state" part of the computation was run for more than 25 cycles of the drive, and so the time differences were the result of averages over 50 estimates.

5. ILLUSTRATIVE CASES

Computations have been performed for four different 25 mm (nominal) Coriolis flow meters, three commercially available meters and a simple straight-tube meter, with tube

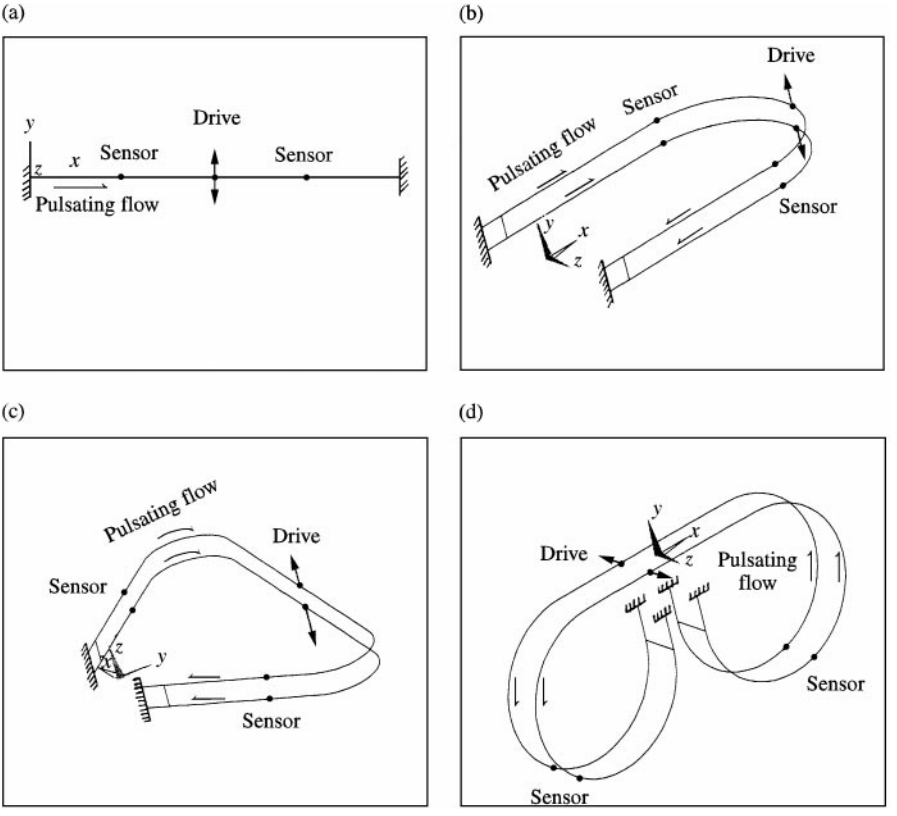

Figure 4. Diagramatic representation of meters models used in computations: (a) straight-tube meter; (b) U-tube meter; (c) Ω-tube meter; (d) B-tube meter.

dimensions based on a commercially available straight meter. The commercial meters comprised: a U-shape dual-tube meter (meter U), a "coat-hanger" shape dual-tube meter (meter Ω) and a B-shape dual-tube meter (meter B). Diagrammatic representations of the meters are shown in Figure 4. The FE representations of the meters were based on dimensions and material properties supplied by the manufacturers, but it should be noted that the FE models do not attempt to represent the additional components attached to the measurement tubes of the commercial meters for the purpose of enhancing their dynamic performance. These are therefore, considerably simplified models. In all the computations the fluid was assumed to be water at ambient temperature.

5.1. Straight-tube Meter

The straight-tube meter was modelled in terms of 29 nodes, it had both ends fixed and was driven at the middle node, see Figure 4. A mean velocity of 6 m/s (mass flow rate 2·6 kg/s) through the meter tube was assumed and a pulsation factor $\alpha = 0{\cdot}1$ was used in the pulsating flow analyses. The natural frequencies of this meter model were $f_1 = 143{\cdot}452$ Hz and $f_2 = 395{\cdot}0$ Hz; this value of f_1 can be compared with that for the no-flow case $f_{1,0} = 143{\cdot}484$ Hz. The difference between f_1 and $f_{1,0}$ agrees with that given by the analysis of Cheesewright and Clark (1998) (C&C). For steady flow, the FE analysis yields a mean time difference between the sensor signals of 9·085 μs as compared with the 8·662 μs given

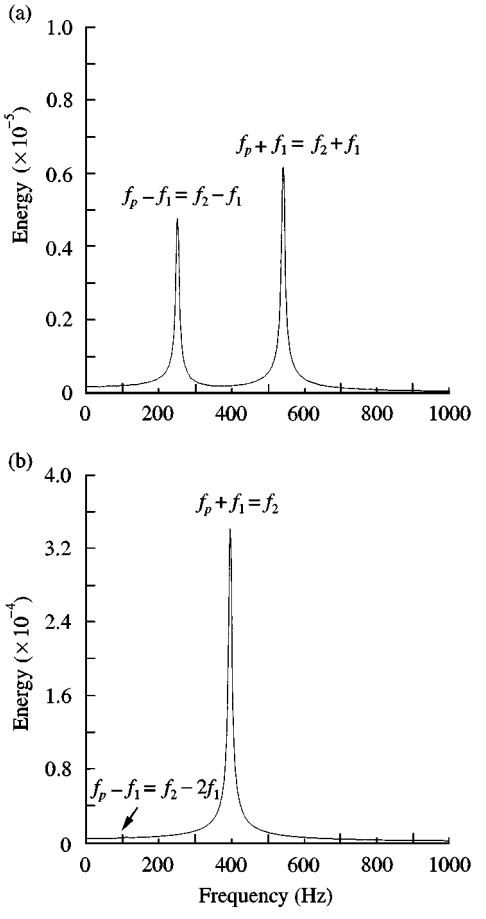

Figure 5. Spectra of simulated sensor signal (drive and Coriolis motions removed): (a) for pulsations at the Coriolis frequency, f_2; (b) for pulsations at difference between the Coriolis frequency and the drive frequency, $f_2 - f_1$ (simple straight-tube meter). Note the differing scales of the ordinates of the two graphs.

by the equation derived by C&C. However, when the FE model was amended to agree more closely with that used by C&C, i.e. Bernoulli beam element, with no axial stresses, etc., the predicted time difference was 8·576 μs, which is in acceptable agreement with the C&C result. The retention of the more complex model in the following FE work, rather than the simpler model used by C&C, is justified on the grounds that it is more realistic, as has been noted by Hulbert, Darnell and Brereton (1995), and the difference is likely to be significant in the geometrically more complex meters.

The effect of flow pulsations is illustrated in Figure 5, where (a) shows the influence of pulsations at the Coriolis frequency, f_2, and (b) shows the influence of pulsations at $f_2 - f_1$. In both cases, the quantity plotted is the spectrum of the difference between the time histories of sensor displacements for flow with and without pulsations (note the differing scales of the ordinates on the two graphs). The peaks in Figure 5(a) are at $f_2 - f_1$ and $f_2 + f_1$, while those in Figure 5(b) are at $(f_2 - f_1) - f_1 = f_2 - 2f_1$ and $(f_2 - f_1) + f_1 = f_2$, with the former of these being only just visible. These peaks are consistent with pulsations having effects at frequencies corresponding to the beat frequencies between pulsation and drive, as

predicted by C&C; and the fact that the peak at f_2 in Figure 5(b) is significantly larger than any of the other peaks is consistent with this being the only peak which is at a system resonant frequency. The absence of spectral peaks at f_1 in Figure 5(a, b) shows that the flow pulsations do not change the proportionality between the phase difference of the components of the sensor signals at f_1 and the mass flow rate. The estimate of the time delay between the two sensor signals for the flow pulsating at f_2 was 9·098 μs, and the difference between this value and the value given above for steady flow (9·084 μs) is less than the uncertainty of the estimates.

The above FE results can be compared with the results from experiments on a commercial straight-tube meter. The two meters are not identical because, although the commercial meter has a straight tube, it is far from simple, and data were not available to model its more complex features. For the same flow rate as used in the model, the commercial meter has a drive frequency of 222 Hz and a Coriolis frequency of 427 Hz. Because of the differences, a direct comparison between the relative amplitudes of FE displacement spectrum and the experimental spectrum was not possible. Hence, the comparison between FE and experimental results is limited to a qualitative examination of the frequency content of the spectra.

Figure 6 shows the power spectrum of a sensor signal from the commercial meter for a flow pulsating at f_2, the corresponding steady flow spectrum, and the difference between the two spectra. Figure 7 shows the corresponding data for a flow pulsating at $f_2 - f_1$. The spectral curves were developed by the periodogram technique using 1·3 s segments (with 50% overlap) from a 4·7 s sensor signal time history. The spectral amplitudes are given in dB relative to the r.m.s. signal voltage. It should be noted that it was not feasible to subtract the time histories of the sensor signals and then derive a spectrum, because the time histories for steady flow and for pulsating flow could not be aligned in time as they could for the

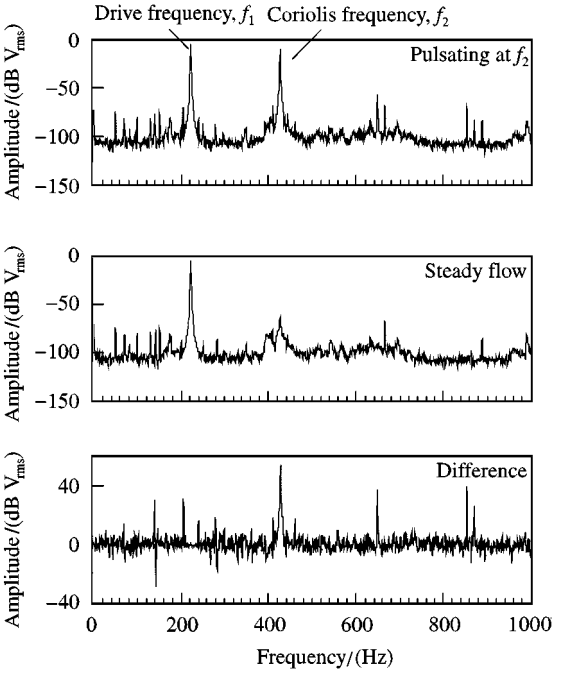

Figure 6. Power spectra of experimental detector signals for pulsations at Coriolis frequency f_2, steady flow, and the difference between the two spectra (commercial straight-tube meter).

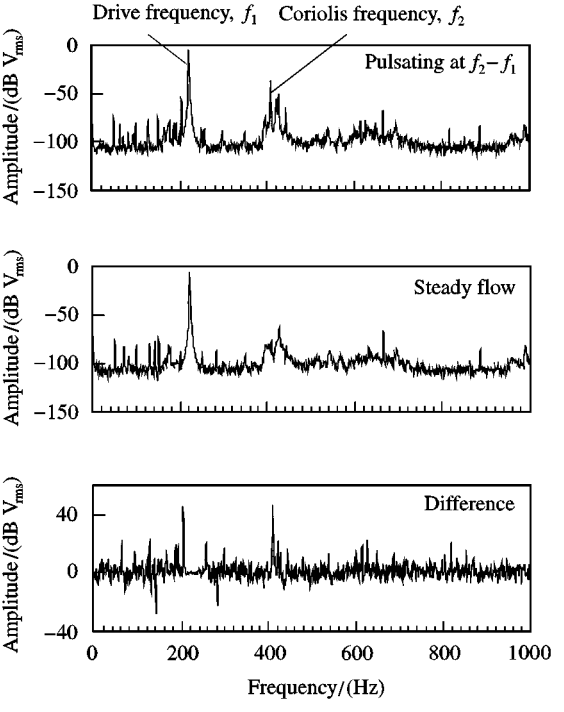

Figure 7. Power spectra of experimental detector signals for pulsations at the difference between the Coriolis frequency and the drive frequency $f_2 - f_1$, steady flow, and the difference between the two spectra (commercial straight-tube meter).

computed time histories. While Figure 6 shows the spectral peaks at $f_2 - f_1 (= 205$ Hz) and $f_2 + f_1 (= 649$ Hz) which appear in Figure 5(a), there is also a significant peak at f_2 and peaks at $2f_2$, $2f_1 + f_2$ and $\sim$140 Hz, which do not appear in Figure 5(a). Cheesewright *et al.* (1999) have recently published convincing evidence that the f_2 peak is due to internal vibrations of the meter, excited by the flow pulsations (a feature which this FE analysis would not be expected to model). The other peaks are most probably due to the more complex features of the meter which were not modelled in the FE analysis.

In the case of a flow pulsating at $f_2 - f_1$ (Figure 7), the frequency component at $f_2 - f_1 + f_1 = f_2 = 427$ Hz is slightly enhanced, there is a significant peak at the pulsation frequency (205 Hz) and also at twice the pulsation frequency (410 Hz). The frequency peak corresponding to $f_2 - f_1 - f_1 = 17$ Hz is not visible, because of its low amplitude (it is not a resonant frequency) and the presence of noise in the signal spectrum. This agrees well with the FE prediction which shows that the amplitude of the component at frequency $f_2 - f_1 - f_1 = f_2 - 2f_1 = 108$ Hz was very small. The significantly smaller amplitude of the peak at f_2 in this case (Figure 7) is worth noting, compared with the previous case (Figure 6), which suggests that the vibration effect due to pulsations could be more important than the direct pulsation effect on meter performance.

5.2. Complex Geometry Meters

To show the application of the FE procedure to meters with more complex geometries, three illustrative examples are presented in what follows. A range of different pulsation frequencies were studied, but, for comparison, it is convenient to concentrate on the case of

the flow pulsation frequency equal to the meter Coriolis frequency f_2, for all three meters. As shown in Figure 4, since all three meters were of the dual tube type, each model was fixed at its ends and was driven at the middle nodes of the two tubes by imposing harmonic displacements having equal amplitudes (0·2 mm) but in anti-phase with each other. The U-tube and the Ω-tube meters were driven in the simple first mode (bending with no twisting, about the z-axis for the U-meter and the x-axis for the Ω-meter), whereas the B-tube was driven at a higher mode (as in the commercial meter), such that the drive and the sensor move in anti-phase with a vibrational node roughly halfway between the driver and each sensor (bending about the x-axis and twisting about the y-axis). A flow pulsation factor α of 0·25 was used for all three meters. Although all three meters were nominally 25 mm in diameter (i.e. they were intended for use in 25 mm diameter pipe systems) the actual flow tubes varied considerably in diameter. The mean flow velocities in each of the two tubes for the different meters were calculated from the cross-sectional areas for a flow rate of 2 kg/s (the flow rate used in the majority of the experiments). This resulted in flow velocities of 7·1, 4·7 and 3·6 m/s, for the U-tube, the Ω-tube and the B-tube, respectively.

The values of the drive and Coriolis frequencies given by the modal analyses of the three meters are reported in Table 1. The presence of two Coriolis frequencies for the B-tube meter results from it being driven at a higher mode (Raszillier & Durst 1991).

Figure 8 (for the U-meter), Figure 9 (for the Ω-meter) and Figure 10 (for the B-meter) show the spectra of the differences between the time histories of displacements at the sensor nodes, with and without flow pulsations, obtained from the analyses of the three meter models. As can be seen, in the case of the U-meter and the Ω-meter, the sensor displacements

TABLE 1

Predicted characteristic frequencies for the U, Ω and B meters

Meter	Drive frequency/(Hz)	Coriolis frequency/(Hz) (upper)	Lower Coriolis frequency/(Hz)
U-meter	78·9	205·0	—
Ω-meter	105·5	178·0	—
B-meter	110·5	186·7	52·8

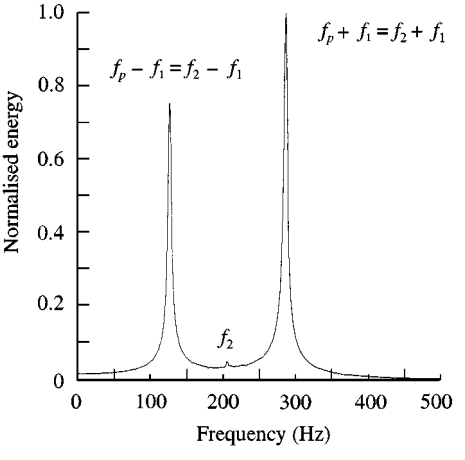

Figure 8. U-tube meter: spectrum of difference between simulated sensor signal with pulsations at the Coriolis frequency, f_2, and the corresponding signal for steady flow.

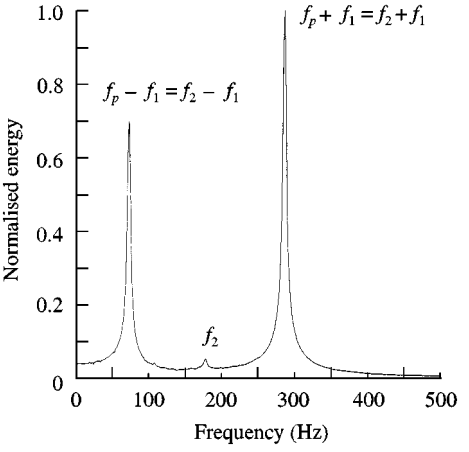

Figure 9. Ω-tube meter: spectrum of difference between simulated sensor signal with pulsations at the Coriolis frequency, f_2, and the corresponding signal for steady flow.

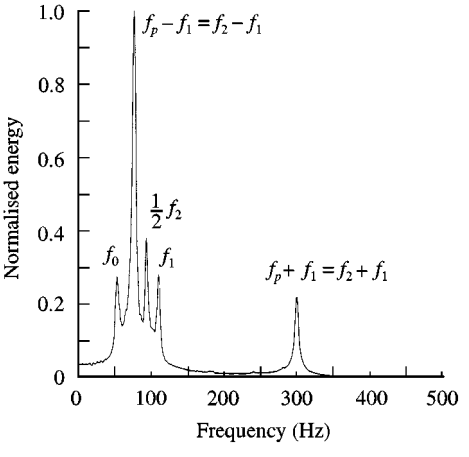

Figure 10. B-tube meter: spectrum of difference between simulated sensor signal with pulsations at the Coriolis frequency, f_2, and the corresponding signal for steady flow.

contain contributions from three frequencies, namely: the Coriolis frequency f_2 and the two frequencies corresponding to the sum of and the difference between the pulsation frequency (f_2) and the drive frequency, i.e. $(f_2 + f_1)$ and $(f_2 - f_1)$, respectively. The small spectral peaks at f_2 are due to initial conditions and would disappear if the FE calculations were run for a longer time. In the case of the B-meter, the spectrum is more complicated; there is no significant peak at f_2, but there are three additional peaks: at frequencies f_0, f_1 and $f_2/2$, where f_0 is the lower Coriolis frequency.

The FE calculations of the response of the B-meter to flow pulsations were constrained by the limitations of computer power, with each simulation taking five to six days to complete. It was thus not clear whether these additional peaks were due to the incomplete damping out of initial conditions, or to the geometrical complexity of the B-meter, or to the fact that it is driven in a higher mode, or to a combination of these factors. In an attempt to establish this dependence, a computation was performed with the B-meter driven in its fundamental mode. Figure 11 shows the equivalent of Figure 10 for this case, and it must be

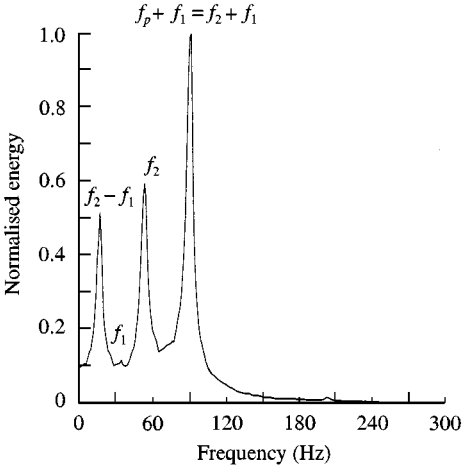

Figure 11. B-tube meter, driven in fundamental mode: spectrum of difference between simulated sensor signal with pulsations at the Coriolis frequency, f_2 and the corresponding signal for steady flow.

noted that the use of f_1 and f_2 to represent the drive frequency and the Coriolis frequency respectively is retained so that the same symbol represents different numerical values of the frequency in the two figures. As might be expected there is no equivalent of the f_0 peak in Figure 11, because there is no lower Coriolis frequency. There were indications that the relatively large f_2 peak in Figure 11 is due to the much slower decay of initial transients at these low (numerical) frequencies and it is expected that it would disappear after a sufficiently long computation. On the assumption that the f_2 peak in Figure 11 is due to a transient effect, there is a clear suggestion that some of the spectral peaks in Figure 10 arise from the meter being driven in a higher mode. However, to establish the definitive response of this complex meter would require the running of the FE model on a faster computer system.

The absence of spectral peaks at f_1 in Figures 5(a, b), 8 and 9 shows that for the straight-tube meter, the U-meter and the Ω-meter, flow pulsations do not affect the linear relationship between the mass flow rate and the phase difference between the f_1 components of the sensor signals. Although Figure 10 for the B-meter shows a small peak at f_1 (which would suggest a change in meter calibration), the amplitude of that peak is approximately 0·05% of the peak for steady flow on which the meter calibration is based. Thus, in view of the limitations reported above on the extent to which the computations for this meter are fully converged, it must be concluded that, although pulsations may produce a change in the calibration of this meter, the change is less than the uncertainty of the meter calibration quoted by the manufacturer.

6. CONCLUSION

A procedure for modelling pulsating flow in Coriolis mass flow meters using a standard FE code has been presented. In the form in which the procedure has been implemented, using the ANSYS FE code, it is easily applicable to any meter geometry and to any meter drive mode. The computations are minimized by using the difference between the two time scales which control meter responses to pulsating flows (drive frequency and pulsation frequency).

The procedure has been validated by comparison with the published analytical solution for a simple straight-tube meter and a comparison with experimental data from

a commercially available straight-tube meter provides a confirmation of the essential features of the computed response.

The procedure has been used to generate the responses of a range of geometrically different, commercially available, meters. These responses show that all meters, regardless of geometry or drive mode, show responses which are characterized by signal components which arise from beating between the pulsation frequency and the meter drive frequency.

The computed responses show that when the meter calibration is expressed in terms of the relationship between the mass flow rate and *the phase difference between the components of the sensor signals at the meter drive frequency*, the calibration is not changed by the presence of flow pulsations. This result shows that the meter errors reported for the measurement of flows with pulsations at the Coriolis frequency of the meter are a result of signal processing and not of the basic meter calibration.

ACKNOWLEDGEMENTS

The authors would like to acknowledge the support of this research by the National Measurement System Policy Unit of the U.K. Department of Trade and Industry (DTI). Thanks are due to the following meter manufacturers for providing meters for experimental work and data on those meters to facilitate the FE representations: ABB, Krohne, and Fisher-Rosemount (Micro Motion).

References

Baker, R. C. 1994 Coriolis flowmeters: industrial practice and published information. *Flow Measurement and Instrumentation* **5,** 229–246.

Bendat, J. S. & Piersol, A. G. 1971 *Random Data*: *Analysis and Measurement Procedures*. New York: Wiley-Interscience.

Cheesewright, R. & Clark, C. 1998 The effect of flow pulsations on Coriolis mass flow meters. *Journal of Fluids and Structures* **12,** 1025–1039.

Cheesewright, R., Clark, C. & Bisset, D. 1999 Understanding the experimental response of Coriolis massflow meters to flow pulsations. *Flow Measurement and Instrumentation* **10,** 207–215.

Hulbert, G. M., Darnell, I. & Brereton, G. J. 1995 Numerical and experimental analysis of Coriolis mass flowmeters. AIAA Technical Paper, AIAA-95-1384-CP.

Misra, A. K., Païdoussis, M. P. & Van, K. S. 1988a On the dynamics of curved pipes transporting fluid. Part I: Inextensible theory. *Journal of Fluids and Structures* **2,** 221–244.

Misra, A. K., Païdoussis, M. P. & Van, K. S. 1988b On the dynamics of curved pipes transporting fluid. Part II: Extensible theory. *Journal of Fluids and Structures* **2,** 245–261.

Olson, L. G. & Jamison, D. 1997 Application of a general purpose finite element method to elastic pipes conveying fluid. *Journal of Fluids and Structures* **11,** 207–222.

Païdoussis, M. P. 1998 *FLUID-STRUCTURE INTERACTIONS*: *Slender Structures and Axial Flow*. London: Academic Press Limited.

Païdoussis, M. P. & Issid, N. T. 1974 Dynamic stability of pipes conveying fluid. *Journal of Sound and Vibration* **33,** 267–294.

Païdoussis, M. P. & Li, G. X. 1993 Pipes conveying fluid: a model dynamical problem. *Journal of Fluids and Structures* **7,** 137–204.

Raszillier, H. & Durst, F. 1991 Coriolis-effect in mass flow metering. *Archives of Applied Mechanics*, **61,** 192–214.

Stack, C.P., Garnett, G. E. & Pawlas, G. E. 1993 A finite element for the vibration analysis of a fluid-conveying Timoshenko beam. *AIAA/ASME Structures, Structural Dynamics and Materials Conference*. AIAA Technical Paper, AIAA-93-1552-CP.

Sultan, G. & Hemp, J. 1989 Modelling of the Coriolis mass flowmeter. *Journal of Sound and Vibration* **132,** 473–489.

Tijsseling, A. S. 1996 Fluid-structure interaction in liquid-filled pipe systems: a review. *Journal of Fluids and Structures* **10,** 109–146.

Vetter, G. & Notzon, S. 1994 Effect of pulsating flow on Coriolis mass flowmeter. *Flow Measurement and Instrumentation* **5,** 263–273.

APPENDIX A: FINITE ELEMENT MATRICES

Assuming that, during each quasi-steady step, the x and t variables are separable, the transverse displacement, flexural rotation and shear strain along the element in each of the (2-D) planes $\{x, y\}$ and $\{x, z\}$ (see Figure 2), can be written in matrix form as (following the procedure of Stack *et al.* 1993):

$$u^{e}_{(x,t)} = N^{T}_{u(x)} q_{(t)} = \left(\frac{1}{1+g}\right) \begin{bmatrix} \left(\frac{2}{L^3}\right)x^3 - \left(\frac{3}{L^2}\right)x^2 - \left(\frac{g}{L}\right)x + g + 1 \\ \left(\frac{1}{L^2}\right)x^3 - \left(\frac{2+0.5g}{L}\right)x^2 + (1+0{\cdot}5g)x \\ \left(\frac{-2}{L^3}\right)x^3 + \left(\frac{3}{L^2}\right)x^2 + \left(\frac{g}{L}\right)x \\ \left(\frac{1}{L^2}\right)x^3 + \left(\frac{-1+0{\cdot}5g}{L}\right)x^2 - 0.5g \end{bmatrix} \times q_{(t)},$$

$$\theta^{e}_{(x,t)} = N^{T}_{\theta(x)} q_{(t)} = \left(\frac{1}{1+g}\right) \begin{bmatrix} \left(\frac{6}{L^3}\right)x^2 - \left(\frac{6}{L^2}\right)x \\ \left(\frac{3}{L^2}\right)x^2 - \left(\frac{4+g}{L}\right)x + 1 \\ \left(\frac{-6}{L^3}\right)x^2 + \left(\frac{6}{L^2}\right)x \\ \left(\frac{3}{L^2}\right)x^2 + \left(\frac{g-2}{L}\right)x \end{bmatrix} \times q_{(t)},$$

$$\phi^{e}_{(x,t)} = N^{T}_{\phi(x)} q_{(t)} = \left(\frac{1}{1+g}\right) \begin{bmatrix} \frac{-g}{L} \\ \frac{-g}{2} \\ \frac{g}{L} \\ \frac{-g}{2} \end{bmatrix} \times q_{(t)}, \tag{A1}$$

where superscript e denotes an element vector, N represents the shape function matrix, T denotes the transpose, q is the nodal displacements and rotations vector, and g is a constant based on material and geometric properties of the meter tube ($= 12EI_p/kGA_PL^2$). The shape functions, which are the same in each plane ($\{x, y\}$ or $\{x, z\}$), are developed based on formulating the static equilibrium of a typical Timoshenko beam, assuming that the transverse displacement follows a cubic variation over the element length (in the plane considered).

When equations (A1) are substituted into equations (1), application of the usual finite element approximations leads to an element equation of motion in the matrix form (for each plane):

$$M\frac{\mathrm{d}^2q}{\mathrm{d}t^2} + B\frac{\mathrm{d}q}{\mathrm{d}t} + Kq = 0, \tag{A2}$$

where the mass matrix, M, the damping matrix B and the stiffness matrix K are defined by

$$M = \int_0^L [(m_p + m_f)N_u^{\mathrm{T}}N_u + (m_p r_p^2 + m_f r_f^2)N_\theta^{\mathrm{T}}N_\theta]\,\mathrm{d}x,$$

$$B = \int_0^t m_f V_0 \left(N_u^{\mathrm{T}}\frac{\mathrm{d}N_u}{\mathrm{d}x} - N_u\frac{\mathrm{d}N_u^{\mathrm{T}}}{\mathrm{d}x}\right)\mathrm{d}x, \tag{A3}$$

$$K = \int_0^L \left(EI_p\frac{\mathrm{d}N_\theta^{\mathrm{T}}}{\mathrm{d}x}\frac{\mathrm{d}N_\theta}{\mathrm{d}x} + kGA_pN_\phi^{\mathrm{T}}N_\phi - m_fV^2\frac{\mathrm{d}N_u^{\mathrm{T}}}{\mathrm{d}x}\frac{\mathrm{d}N_u}{\mathrm{d}x} - m_f\frac{\mathrm{d}V}{\mathrm{d}t}(L-x)\frac{\mathrm{d}N_u^{\mathrm{T}}}{\mathrm{d}x}\frac{\mathrm{d}N_u}{\mathrm{d}x}\right)\mathrm{d}x.$$

The global 3-D element matrices are then readily written by the superposition of the flexural matrices (in the $\{x, y\}$ and $\{x, z\}$ planes) and the axial and torsional matrices for a standard beam (in the $\{y, z\}$ plane). The resulting matrices are given by the following:
mass matrix:

$$M = \begin{bmatrix}
M_3 & & & & & & & & & & & \\
0 & m_{11} & & & & & & & & & & \\
0 & 0 & m_{11} & & & & & & & & & \\
0 & 0 & 0 & M_a & & & & & & & & \\
0 & 0 & -m_{21} & 0 & m_{22} & & & \text{Symmetric} & & & & \\
0 & m_{21} & 0 & 0 & 0 & m_{22} & & & & & & \\
M_6 & 0 & 0 & 0 & 0 & 0 & M_3 & & & & & \\
0 & m_{31} & 0 & 0 & 0 & m_{32} & 0 & m_{33} & & & & \\
0 & 0 & m_{31} & 0 & -m_{32} & 0 & 0 & 0 & m_{33} & & & \\
0 & 0 & 0 & M_b & 0 & 0 & 0 & 0 & 0 & M_a & & \\
0 & 0 & m_{41} & 0 & m_{42} & 0 & 0 & 0 & m_{43} & 0 & m_{44} & \\
0 & -m_{41} & 0 & 0 & 0 & m_{42} & 0 & -m_{43} & 0 & 0 & 0 & m_{44}
\end{bmatrix}; \tag{A4a}$$

damping matrix:

$$B = \begin{bmatrix}
0 & & & & & & & & & & & \\
0 & 0 & & & & & & & & & & \\
0 & 0 & 0 & & & & & & & & & \\
0 & 0 & 0 & 0 & & & & & & & & \\
0 & 0 & -b_{21} & 0 & 0 & & & \text{Anti-symmetric} & & & & \\
0 & b_{21} & 0 & 0 & 0 & 0 & & & & & & \\
0 & 0 & 0 & 0 & 0 & 0 & 0 & & & & & \\
0 & b_{31} & 0 & 0 & 0 & b_{32} & 0 & 0 & & & & \\
0 & 0 & b_{31} & 0 & -b_{32} & 0 & 0 & 0 & 0 & & & \\
0 & 0 & 0 & 0 & 0 & 0 & 0 & 0 & 0 & 0 & & \\
0 & 0 & -b_{41} & 0 & b_{42} & 0 & 0 & 0 & -b_{43} & 0 & 0 & \\
0 & b_{41} & 0 & 0 & 0 & b_{42} & 0 & b_{43} & 0 & 0 & 0 & 0
\end{bmatrix}; \tag{A4b}$$

stiffness matrix:

$$K = \begin{bmatrix} K_a & & & & & & & & & & & \\ 0 & k_{11} & & & & & & & & & & \\ 0 & 0 & k_{11} & & & & & & & & & \\ 0 & 0 & 0 & K_t & & & & & & & & \\ 0 & 0 & -k_{21} & 0 & k_{22} & & & \text{Symmetric} & & & & \\ 0 & k_{21} & 0 & 0 & 0 & k_{22} & & & & & & \\ -K_a & 0 & 0 & 0 & 0 & 0 & K_a & & & & & \\ 0 & -k_{11} & 0 & 0 & 0 & k_{32} & 0 & k_{33} & & & & \\ 0 & 0 & -k_{11} & 0 & -k_{32} & 0 & 0 & 0 & k_{33} & & & \\ 0 & 0 & 0 & -K_t & 0 & 0 & 0 & 0 & 0 & K_t & & \\ 0 & 0 & -k_{41} & 0 & k_{42} & 0 & 0 & 0 & -k_{43} & 0 & k_{44} & \\ 0 & k_{41} & 0 & 0 & 0 & k_{42} & 0 & k_{43} & 0 & 0 & 0 & k_{44} \end{bmatrix}; \tag{A4c}$$

where

$$m_{11} = m_{33} = \frac{(m_p + m_f)L}{(1+g)^2}\left(\frac{1}{3}g^2 + \frac{7}{10}g + \frac{13}{35}\right) + \frac{6L}{5(1+g)^2}\left[m_p\left(\frac{r_p}{L}\right)^2 + m_f\left(\frac{r_f}{L}\right)^2\right],$$

$$m_{21} = -m_{43} = \frac{(m_p + m_f)L^2}{(1+g)^2}\left(\frac{1}{24}g^2 + \frac{11}{120}g + \frac{11}{210}\right) + \frac{(1-5g)L^2}{10(1+g)^2}\left[m_p\left(\frac{r_p}{L}\right)^2 + m_f\left(\frac{r_f}{L}\right)^2\right],$$

$$m_{22} = m_{44} = \frac{(m_p + m_f)L^3}{(1+g)^2}\left(\frac{1}{120}g^2 + \frac{1}{60}g + \frac{1}{105}\right) + \frac{(4 + 5g + 10g^2)L^3}{30(1+g)^2}\left[m_p\left(\frac{r_p}{L}\right)^2 + m_f\left(\frac{r_f}{L}\right)^2\right],$$

$$m_{31} = \frac{(m_p + m_f)L}{(1+g)^2}\left(\frac{1}{6}g^2 + \frac{3}{10}g + \frac{9}{70}\right) - \frac{6L}{5(1+g)^2}\left[m_p\left(\frac{r_p}{L}\right)^2 + m_f\left(\frac{r_f}{L}\right)^2\right],$$

$$m_{32} = m_{41} = \frac{(m_p + m_f)L^2}{(1+g)^2}\left(\frac{1}{24}g^2 + \frac{3}{40}g + \frac{13}{420}\right) - \frac{(1-5g)L^2}{10(1+g)^2}\left[m_p\left(\frac{r_p}{L}\right)^2 + m_f\left(\frac{r_f}{L}\right)^2\right],$$

$$m_{42} = \frac{(m_p + m_f)L^3}{(1+g)^2}\left(\frac{1}{120}g^2 + \frac{1}{60}g + \frac{1}{140}\right) + \frac{(1 + 5g - 5g^2)L^3}{30(1+g)^2}\left[m_p\left(\frac{r_p}{L}\right)^2 + m_f\left(\frac{r_f}{L}\right)^2\right], \tag{A5}$$

$$M_1 = \frac{1}{3}(m_p + m_f)L, \quad M_6 = \frac{M_3}{2}, \quad M_a = \frac{J_p}{3A_p}(m_p + m_f)L, \quad M_b = \frac{M_a}{2},$$

$$b_{21} = b_{32} = -b_{41} = b_{43} = \left(\frac{Lm_fV}{60} \times \frac{6 + 5g}{1+g}\right),$$

$$b_{31} = -0{\cdot}5m_f V, \quad b_{42} = \frac{L^2 m_f V}{60(1+g)},$$

$$k_{11} = -k_{31} = k_{33} = \frac{12EI_p}{L^3(1+g)} - \frac{10g^2+20g+12}{(1+g)}\left(\frac{m_f V^2}{10L} + \frac{m_f}{20}\frac{\mathrm{d}V}{\mathrm{d}t}\right),$$

$$k_{21} = -k_{12} = k_{41} = -k_{43} = \frac{6EI_p}{L^2(1+g)} - \frac{1}{(1+g)^2}\frac{m_f V^2}{10} + \frac{m_f L(5g^2+8g)}{60(1+g)^2}\frac{\mathrm{d}V}{\mathrm{d}t},$$

$$k_{42} = \frac{EI_p(2-g)}{L(1+g)} + \frac{30g^2+60g+12}{(1+g)^2}\left(\frac{m_f L V^2}{360} + \frac{m_f L^2}{720}\frac{\mathrm{d}V}{\mathrm{d}t}\right),$$

$$k_{22} = k_{44} = \frac{EI_p(4+g)}{L(1+g)} - \frac{45g^2+90g+72}{(1+g)^2}\left(\frac{m_f L V^2}{540}\right) - \frac{15g^3+42g+36}{(1+g)^2}\left(\frac{m_f L^2}{360}\frac{\mathrm{d}V}{\mathrm{d}t}\right),$$

$$K_a = \frac{EI_p}{L}, \quad K_t = \frac{GJ_p}{L}.$$

Note. When the above matrix elements were used in the transient FE computations, the terms involving the fluid velocity ($V = V_0(1 + \alpha \sin \omega_p t)$) were separated into steady and time-dependent parts.

APPENDIX B: NOMENCLATURE

A_p	tube wall cross-sectional area
A_f	fluid cross-sectional area
B	damping matrix
E	tube modulus of elasticity
f_0	lower Coriolis frequency (for a meter not driven at first mode)
f_1	meter drive frequency
$f_{1,0}$	meter frequency with no flow, i.e. for $V = 0$.
f_2	meter Coriolis frequency (second mode for straight-tube meter driven at first mode; upper Coriolis frequency for a meter *not* driven at first mode)
f_p	flow pulsation frequency
G	tube shear modulus
I_p	moment of inertia/length, of tube cross-section about the central axis
I_f	moment of inertia/length, of fluid about the central axis
q	vector of nodal displacements and rotations
J_p	tube torsional moment of inertia $= 2I_p$
k	Timoshenko shear coefficient, dependent on shape of tube cross-section ($k = 0{\cdot}5$ for circular cross-section tube)
K	stiffness matrix
L	length of the straight-tube meter
$\dot{m}_f$	fluid mass flow rate $= \rho_f A_f V$
m_p	mass of tube per length $= \rho_p A_p$
m_f	mass of fluid per length of tube $= \rho_f A_f$
M	mass matrix
r_p	tube radius of gyration $= \sqrt{I_p/A_p}$
r_f	fluid radius of gyration $= \sqrt{I_f/A_f}$
t	time
T_p	flow velocity pulsation period
u	transverse displacement $= u(x, t)$

V fluid velocity
V_0 mean fluid velocity
x distance along tube element axis
α pulsation factor (<1)
γ_1 meter first mode circular frequency $= 2\pi f_1$
γ_2 meter Coriolis circular frequency $= 2\pi f_2$
Δt analysis time step
Δt_s time shift between sensor signals
Δt_p fluid velocity sampling time interval
θ flexural rotation $= \theta(x, t)$
ρ_p tube density
ρ_f fluid density
ϕ shear strain $= \phi(x,t) = \partial u/\partial x - \theta$
ω_p pulsation circular frequency $= 2\pi f_p$